

Metal-Organic Capsules with NADH Mimics as Switchable Selectivity Regulators for Photocatalytic Transfer Hydrogenation

Jianwei Wei, Liang Zhao, Cheng He, Sijia Zheng, Joost N. H. Reek, and Chunying Duan

J. Am. Chem. Soc., **Just Accepted Manuscript** • DOI: 10.1021/jacs.9b05351 • Publication Date (Web): 18 Jul 2019

Downloaded from pubs.acs.org on July 19, 2019

Just Accepted

“Just Accepted” manuscripts have been peer-reviewed and accepted for publication. They are posted online prior to technical editing, formatting for publication and author proofing. The American Chemical Society provides “Just Accepted” as a service to the research community to expedite the dissemination of scientific material as soon as possible after acceptance. “Just Accepted” manuscripts appear in full in PDF format accompanied by an HTML abstract. “Just Accepted” manuscripts have been fully peer reviewed, but should not be considered the official version of record. They are citable by the Digital Object Identifier (DOI®). “Just Accepted” is an optional service offered to authors. Therefore, the “Just Accepted” Web site may not include all articles that will be published in the journal. After a manuscript is technically edited and formatted, it will be removed from the “Just Accepted” Web site and published as an ASAP article. Note that technical editing may introduce minor changes to the manuscript text and/or graphics which could affect content, and all legal disclaimers and ethical guidelines that apply to the journal pertain. ACS cannot be held responsible for errors or consequences arising from the use of information contained in these “Just Accepted” manuscripts.

Metal-Organic Capsules with NADH Mimics as Switchable Selectivity Regulators for Photocatalytic Transfer Hydrogenation

Jianwei Wei,[†] Liang Zhao,^{*,†} Cheng He,[†] Sijia Zheng,[†] Joost N. H. Reek,[‡] and Chunying Duan^{*,†}

[†]State Key Laboratory of Fine Chemicals, Zhang Dayu College of Chemistry, Dalian University of Technology, Dalian 116024, People's Republic of China.

[‡]Van't Hoff Institute for Molecular Sciences, University of Amsterdam, Science Park 904, Amsterdam 1098XH, The Netherlands.

ABSTRACT: Switchable selective hydrogenation among the groups in multifunctional compounds is challenging, because selective hydrogenation is of great interest in the synthesis of fine chemicals and pharmaceuticals due to the importance of key intermediates. Herein, we report a new approach for highly selectively (> 99%) reducing C=X (X = O, N) over the thermodynamic more favorable nitro groups by location of the substrate in a metal-organic capsule containing NADH active sites. Within the capsule, the NADH active sites reduce the double bonds *via* a typical $2e^-$ hydride transfer hydrogenation, and the formed excited-state NAD^+ mimics oxidize the reductant *via* two consecutive $1e^-$ processes to regenerate the NADH active sites under illumination. Outside the capsule, nitro groups are highly selectively reduced through a typical $1e^-$ hydrogenation. By combining photoinduced $1e^-$ transfer regeneration outside the cage, both the $1e^-$ and $2e^-$ hydrogenation can be switched controllably by varying the concentrations of the substrates and the redox potential of electron donors. This promising alternative approach, which could proceed under mild reaction conditions and use easy-to-handle hydrogen donors with enhanced high selectivity towards different groups, is based on the localization and differentiation of the $2e^-$ and $1e^-$ hydrogenation pathways inside and outside the capsules and provides a deep comprehension of photocatalytic microscopic reaction processes and will allow the design and optimization of catalysts. We demonstrate the advantage of this method over typical hydrogenation that involves specific activation *via* well-modified catalytic sites and present results on the high, well-controlled and switchable selectivity for the hydrogenation of a variety of substituted and bifunctional aldehydes, ketones and imines.

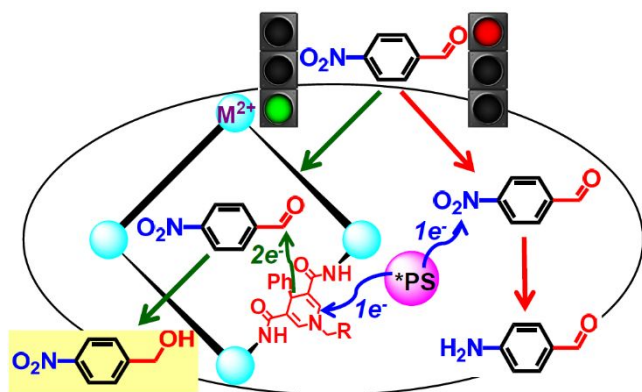
INTRODUCTION

Transfer hydrogenation reactions that proceeds under mild reaction conditions with easy-to-handle hydrogen donors instead of hydrogen gas, is a rapidly growing field as it facilitates the practical synthesis of fine chemicals using complicated compounds with multiple functional groups.¹⁻⁴ Recent breakthroughs in transfer hydrogenation have enabled selective transformations of ketones^{5,6} and aldehydes^{7,8} into their corresponding alcohols in the presence of other functional groups, including the thermodynamic more favorable hydrogenation group, such as nitroarenes and olefins. However, the direct activation of specific groups using well-modified catalytic sites precludes practically inverting and switching the selectivity of the hydrogenation in bifunctional compounds in a single catalytic process. A strategy to selective hydrogenation was proposed, which involves differentiation of $2e^-$ (hydride) and $1e^-$ hydrogenation pathways. The hydride $2e^-$ transfer hydrogenation of ketones and aldehydes over substrates typically hydrogenated *via* $1e^-$ transfer pathways.⁹ Of particular interest is the $2e^-$ hydride transfer hydrogenation using the redox cofactor NADH (reduced nicotinamide adenine nucleotide) and its mimics¹⁰ based on its central role as a cosubstrate in biosynthetic pathways and the potential of NADH to serve as a hydride source while being a weak single-electron reductant.^{11,12} Therefore, new synthetic platforms in which the selectivity in transformations of bifunctional compounds could be strictly controlled and readily tuned by regulating the reaction kinetics of the hydrogenation

pathways involving NADH, such as those involving natural enzymes, may facilitate the selective preparation of fine chemicals and pharmaceuticals bearing multiple functional groups.

To mimic remarkable abilities of enzymes to achieve efficient chemical conversions, researchers have used various molecular capsules, including symmetric metal-organic capsules with defined hydrophobic cavities that are spontaneously generated through preorganized ligands and functionalized metallocorners, as promising hosts to catalyze unique chemical transformations.¹³⁻¹⁶ Reactions performed in such molecular capsules could be enhanced by proximity effects with allowing unusual selectivity and unique dynamics owing to the restricted motion of the substrates. Recently, it was demonstrated that capsules can be used to separate redox events, exploiting the difference between the inner and outer spaces of a host to combine photocatalytic proton reduction and substrate oxidization in a one-pot transformation.^{17,18} Artificial enzymatic systems that combine photocatalytic chemical transformations, including the proton reduction, to regenerate the active sites in NADH mimics and biomimetic hydrogenation reactions have also been postulated as a new synthetic platform.¹⁹⁻²¹ The localization of $2e^-$ hydride transfer hydrogenation pathway inside the reaction vessel containing the NADH mimics thus allow the design and optimization of catalysts, which could proceed under mild reaction conditions and use easy-to-handle hydrogen donors with enhanced high selectivity.

Scheme 1 Schematic of switching the transfer hydrogenation selectivity inside and outside the pocket of the capsule. The *PS represents the excited-state photosensitizer.



We herein report a molecular flask with NADH type cofactors that allows to control the selectivity of a photocatalytic transfer hydrogenation reaction, toggling between a carbonyl or nitro group reduction in bifunctionalized compounds under mild reaction conditions (Scheme 1). Substrate binding in the molecular flask results in pre-organization and thus facilitates the typical $2e^-$ hydride transfer hydrogenation which is highly selective for the carbonyl, whereas the $1e^-$ transfer hydrogenation events takes place when the substrate is outside the molecular flask. We envisioned that with this approach, aldehyde and ketone groups could be highly selectively hydrogenated in presence of nitro group that are the thermodynamic more favorable to convert. These active NADH mimics could be regenerated from the formed NAD^+ mimics *via* oxidation of the reductant through two consecutive $1e^-$ reduction processes under illumination. Outside the pocket, a typical $1e^-$ transfer hydrogenation environment was modified by the presence of a reductant or photosensitizer to highly selectively reduce the nitro group over the carbonyl group. Notably, both hydrogenation processes are well controlled by strictly limiting the different electron transfer pathways to inside and outside the molecular host. The selectivity of hydrogenation of bifunctional compounds could be inverted by simply regulating the reaction kinetics of the two hydrogenation pathways, *i.e.*, varying the concentrations of the substrate and electron donor, because the kinetics inside the pocket are controlled only by the concentration of the host-guest complex and not directly by the concentration of the substrate.

RESULTS AND DISCUSSION

Preparation and characterization of macrocycles and host-guest complex. The ligand H_2FPB was synthesized by a Schiff-base reaction of 2-pyridylaldehyde and 1-(furan-2-ylmethyl)-4-phenyl-1,4-dihydropyridine-3,5-dicarbohydrazide in an ethanol solution. The M_4L_4 metal-organic macrocycles were prepared by reacting the ligand H_2FPB with the appropriate metal salts in acetonitrile solution. Diffraction grade single crystals of the macrocycles including Zn-FPB , Fe-FPB , Co-FPB and Ni-FPB were obtained by vapor diffusion of diethyl ether into the corresponding CH_3CN solutions of the macrocycles (Figures 1a, 1b and S1–S4).

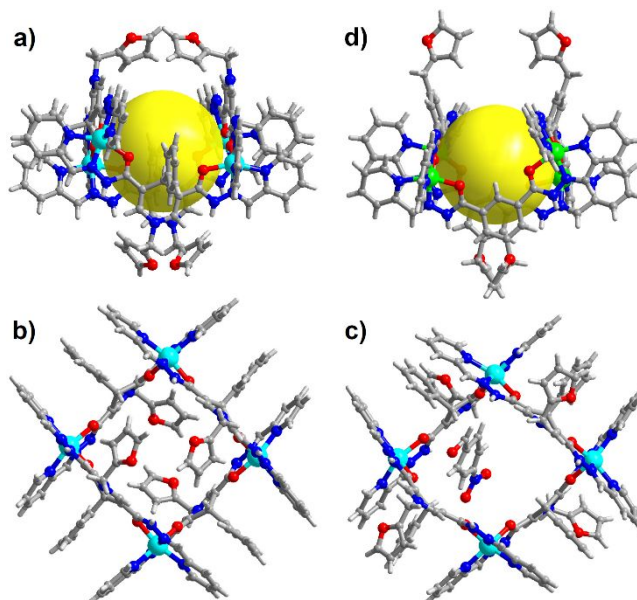


Figure 1. Crystal structures of the macrocycle Zn-FPB (a) with NADH-mimicking ligands showing the coordination geometry of the zinc ions and top view (b) of the macrocycle showing the resulting confined space. Crystal structures of the host-guest complex $\text{Zn-FPB} \supset \mathbf{1}$ (c) and macrocycle Ni-FPB (d) without NADH-mimicking ligands. Anions and solvent molecules are omitted for clarity. Zn cyan, Ni green, O red, N blue, C grey and H white.

Single-crystal structure analyses revealed that the four macrocycles are isostructural and exhibit S_4 symmetry *via* the connection of four ligands with the dihydropyridine amido (**DHPA**) fragments and four metal ions in an alternating fashion.²² The four **DHPA** moieties are positioned on parallel edges of the molecular square with the phenyl ring outside of the cavity and the four active H atoms in the pocket interior.²³ Given the van der Waals radii (3.6 Å) of the guest molecules and the edges of the square, the average $\text{Zn}\cdots\text{Zn}$ separation of approximately 8.62 Å suggests that the cavity of the square is sufficiently large to encapsulate planar aromatic substrate. Each zinc ion was coordinated in a *mer* position with a pair of extensively delocalized N_2O chelators to ensure the mobility of electrons along the whole backbone of the ligands. Such electrons have the potential to migrate from the metal centres to the active sites of the NAD^+ models, enabling the regeneration of the active sites from the photoreduced redox reaction involving the metal ions. The four furan rings are positioned above and below the molecular square to form a pocket for guest inclusion. Importantly, the host-guest complex $\text{Zn-FPB} \supset \mathbf{1}$ (4-nitrobenzaldehyde) was obtained by the same method, which provided unambiguous evidence for the complex formation (Figures 1c and S5). Single-crystal structure analysis shows one guest molecule **1** binds in the pocket.²⁴ The main structure of the molecular square is maintained with the furan rings twisting in the lateral direction. The shortest interatomic distance between **1** and the host structure is 3.52 Å.²⁵ Moreover, the molecule structures of both Zn-FPB and host-guest complex $\text{Zn-FPB} \supset \mathbf{1}$ determined from DFT calculation were good consistent with their single-crystal structures (Figure S19).²⁶ There is close proximity between the active hydrides of the host and **1**, providing the possibility to stabilize the structurally confined intermediate for potential size- and shape- selective hydrogenation.²⁷

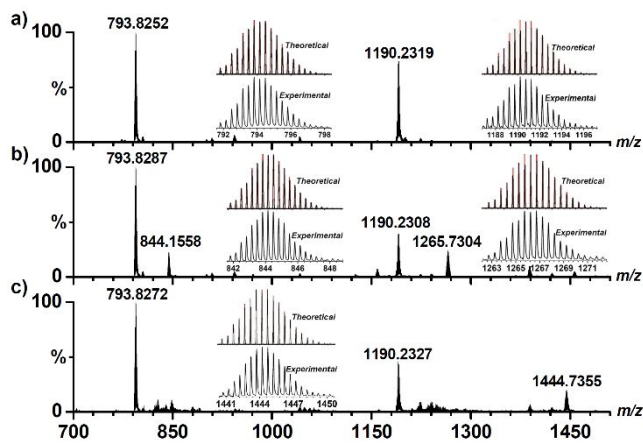


Figure 2. ESI-MS spectra of Zn-FPB (a), Zn-FPB (b) following the addition of 5 equiv. of substrate **1** and Zn-FPB (c) following the addition of 5 equiv. of inhibitor ATP in CH₃CN. The insets show the measured and simulated isotopic patterns at $m/z = 793.83, 844.16, 1190.23, 1265.73$ and 1444.74 .

The structure stability of Zn-FPB in solution was further characterized by ESI-MS spectra that exhibited two sharp peaks at $m/z = 793.83$ and 1190.23 with the exact distribution fingerprint of the $[H_3Zn_4(FPB)_4]^{3+}$ and $[H_2Zn_4(FPB)_4]^{2+}$ species, respectively (Figure 2a). Guest binding in the pocket of the host is evident by ESI-MS analysis of a mixture of the molecular macrocycle

Table 1. Evaluation of hydrogenation for different types of unsaturated groups and unsaturated groups containing electronic pushing and drawing substituents with Zn-FPB.^a

No.	Substrates	Potential (eV)	Yield (%)	No.	Substrates	Potential (eV)	Yield (%)	No.	Substrates	Potential (eV)	Yield (%)
2		-1.31	Trace	7		-1.29	87	12		-1.06	Trace
3		-1.42	86	8		-1.61	75	13		-1.19	Trace
4		-1.68	47	9		-1.66	57	14		-1.36	Trace
5		-1.75	36	10		-1.79	26	15		-1.46	Trace
6		-2.62	Trace	11		-1.88	28	16		-1.49	Trace

^aReaction conditions: Substrate (10.0 mM), Zn-FPB (10.0 mM) and NaBH₃CN (10.0 mM) in CH₃CN/H₂O solution (1:1, 5mL), 6h. The conversions were determined by ¹H NMR spectroscopy of crude products. The redox potentials of substrates were determined by cyclic voltammogram of the 1.0 mM CH₃CN/H₂O solution containing 0.1 M KCl. Scan rate: 100 mV/s.

Zn-FPB and **1** that shows the appearance of two new peaks that correspond to the $[H_3Zn_4(FPB)_4(1)]^{3+}$ and $[H_2Zn_4(FPB)_4(1)]^{2+}$ species at $m/z = 844.16$ and 1265.73 , respectively. A comparison of the experimental peaks with that obtained *via* simulation based on natural isotopic abundances suggested the formation of a 1:1 stoichiometric species, Zn-FPB ⊃ **1**, in solution (Figure 2b).

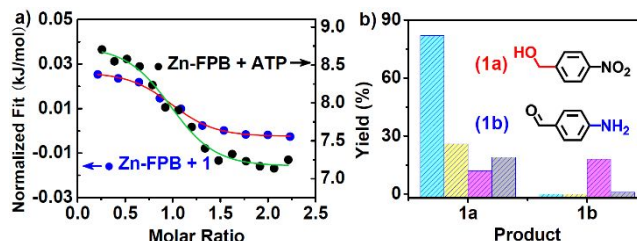


Figure 3. (a) ITC experiments on Zn-FPB upon the addition of substrate **1** or ATP showing the formation of host-guest complexes in CH₃CN. (b) Yields of (cyan bars) 4-nitrophenyl methanol (**1a**) and 4-aminobenzaldehyde (**1b**) by the system containing substrate **1** (5.0 mM), Zn-FPB (0.1 mM), NaBH₃CN (1.0 mM) and HCOOH/Et₃N (0.1 M/0.05 M) in a CH₃CN/H₂O solution (1:1, pH = 8.50) for 6h under 420 nm. The magenta, yellow and grey bars show the yields of **1a** and **1b** in the presence of the ATP (25.0 mM, yellow bars), benzoquinone (5.0 mM, magenta bars) and TEMPO (5.0 mM, grey bars).

Further characterization of the host-guest complex comes from isothermal titration calorimetry (ITC) experiments, of which the spectrum fit well to a 1:1 binding model, providing both the enthalpy ($\Delta H = 0.03$) and entropy ($T\Delta S = 24.83 \text{ kJ}\cdot\text{mol}^{-1}$) of formation of the complex Zn-FPB ⊃ **1** with association constant $2.21 \times 10^4 \text{ M}^{-1}$ (Figures 3a and S11).²⁸ The formation of the host-guest complex is also evident from the fluorescence titration (Figure S21) and the change in chemical shifts in the ¹H NMR

spectra of both the substrate and molecular square (Figure S14). In addition, NOE contacts between the benzene rings of **1** and the NADH mimics of the molecular macrocycle were observed in the NOESY spectrum of the host-guest complex Zn-FPB ⊃ **1** (Figure S15), which suggest that **1** is in close contact with the host when bound in the macrocycle.²⁹ These results indicate that the formation of the host-guest complex pre-organized for efficient substrate activation.^{30,31}

Highly selective photocatalytic transfer hydrogenation. The activity of the macrocycle catalyst Zn-FPB was first studied by chemical reduction of the different types of double bond (carbonyl, imine, olefin and nitro). The substrates containing the

double bonds C=N and C=O can be stoichiometrically reduced by Zn-FPB through the $2e^-$ hydride transfer hydrogenation in the presence of NaBH_3CN ³² and yield increases with the increase of substrate potential (Table 1). In the presence of an electron withdrawing group, the conversion of the transfer hydrogenation significantly increased, whereas an electron donating group significantly decreased the benzaldehyde conversion. However, neither an electron withdrawing nor donating group changed the reactivity of nitrobenzene as it stayed inert for the $2e^-$ transfer hydrogenation, even though reduction of the nitro group is thermodynamically more favorable than the reduction of the carbonyl group.

In the model reaction of substrate **1** (5.0 mM) containing both nitro and aldehyde groups, Zn-FPB stoichiometrically yielded product **1a** (4-nitrophenylmethanol, 91%) with over 99% selectivity. Localizing the electron donors, *i.e.*, $\text{HCOOH}/\text{Et}_3\text{N}$, outside the capsules to *in situ* regenerate the active sites of the NADH mimics^{33,34} allowed Zn-FPB to operate as an efficient catalyst and achieve highly selective hydrogenation under light illumination. While the ground state NAD^+ mimics is a weak single electron oxidant, the excited state NAD^+ mimics is a strong oxidant that is able to get two electrons consecutively from the reductant in the solution, quickly regenerating the active NADH mimics. The loading of Zn-FPB (0.1 mM) resulted in 82% conversion of **1a** with a selectivity of 98% after 6h under 420 nm LED light illumination and the conversion of the thermodynamically favored hydrogenation product **1b** (4-aminobenzaldehyde) is less than 1% (Figure 3b). The results indicate that our approach of localizing the NADH-cofactor-derived biomimetic $2e^-$ hydride transfer hydrogenation pathway to control the selectivity is feasible.

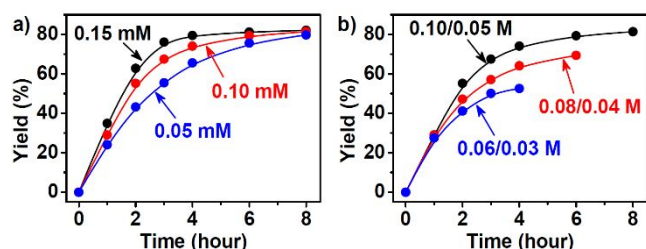


Figure 4. Kinetics of the hydrogenation reaction by the system containing (a) substrate **1** (5.0 mM), $\text{HCOOH}/\text{Et}_3\text{N}$ (0.1/0.05 M) and NaBH_3CN (1.0 mM) with different concentrations of Zn-FPB; (b) substrate **1** (5.0 mM), Zn-FPB (0.1 mM) and NaBH_3CN (1.0 mM) with different concentrations of $\text{HCOOH}/\text{Et}_3\text{N}$ in a $\text{CH}_3\text{CN}/\text{H}_2\text{O}$ solution (1:1, pH = 8.50) under 420 nm illumination.

Control experiments using the related salts and ligands yielded a trace of the product under the same conditions, confirming that the supermolecular host to pre-organize the substrate is essential. When the concentrations of $\text{HCOOH}/\text{Et}_3\text{N}$ and **1** are fixed, the initial rate constant for hydrogenation exhibited a linear relationship with the concentration of Zn-FPB (Figure 4a). When the concentrations of **1** and Zn-FPB are fixed, the initial turnover frequency of hydrogenation did not vary with the concentration of $\text{HCOOH}/\text{Et}_3\text{N}$, but the conversion of **1** increased (Figure 4b). The dependence of the reaction rate on the host-guest concentration of the Zn-FPB \supset **1** species rather than the concentration of **1** or the electron donor is in line with a mechanism in which the reaction occurs within the pocket of Zn-FPB (Figure S16).³⁵ In line with this, the use of a substrate with bulky substituents **17** (3,5-bis(4-nitrophenyl)benzaldehyde), which is too large to fit in the cavity

of Zn-FPB, yielded only 17% of the desired product under the same conditions.

We wondered if we could also switch the catalyst properties by binding a competing guest in the host.³⁶ Adenosine triphosphate (ATP) has similar width with **1**, which is smaller than the inner space of the pocket in Zn-FPB. Importantly, two negative charges and multiple hydrogen bonding sites endow ATP with larger binding constants than that of neutral substrates for the positively charged Zn-FPB. And ATP that is inactive toward hydrogenation, was usually chosen as a competitive guest introducing into the system.³⁷ ITC result shows a 1:1 encapsulation of ATP within the pocket of Zn-FPB (Figures 3a and S12) with ΔH (1.76 $\text{kJ}\cdot\text{mol}^{-1}$), $T\Delta S$ (31.4 $\text{kJ}\cdot\text{mol}^{-1}$) and association constant ($1.58 \times 10^5 \text{ M}^{-1}$).²⁸ And this result was further determined by fluorescence titration (Figure S22), which showed a higher affinity than that of **1** for the host. Moreover, ITC titration was further tested by addition of ATP into a solution of Zn-FPB and **1** (1:1) complex and was fitted well using a 'competitive replacement' model (Figure S13),^{38,39} providing the association constant $3.07 \times 10^4 \text{ M}^{-1}$ and $1.59 \times 10^5 \text{ M}^{-1}$ with **1** and ATP, respectively, which was good consistent with previous data. The results further confirmed that ATP was a good competitive guest for encapsulating into the cavity of Zn-FPB to replace substrate **1**. When the addition of ATP (25.0 mM) into aforementioned catalytic system, the formation of complexes Zn-FPB \supset ATP was over 90% ($K_{\text{ATP}}[\text{ATP}] > 25K_{\text{sub}}[\text{sub}]$) in the reaction condition. Indeed, a catalysis experiment using **1** as substrate, in the presence of ATP (25.0 mM) caused a significant decrease in the yield of **1a** (82%, *c.f.* 26%) compared to the reaction in absence of ATP (Figure 3b). This shows that the ATP effectively competes with **1** for binding in the pocket, and as such the catalyst properties can be controlled by using this as cofactor.⁴⁰

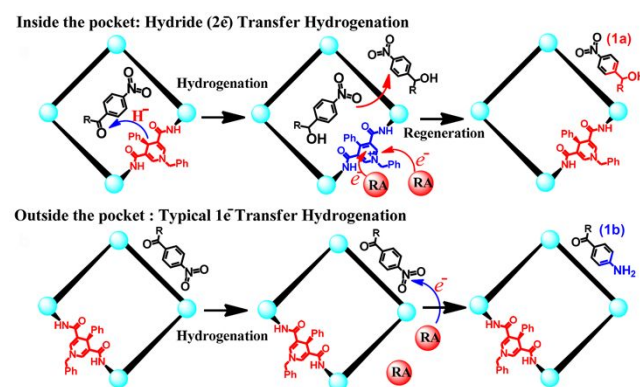


Figure 5. Schematic picture of transfer hydrogenation reactions taking place inside the host and outside, leading to different chemo-selectivity. When the substrate is in the pocket, the $2e^-$ hydride transfer hydrogenation reaction with the NADH cofactor of the molecular host results in carbonyl reduction, whereas the reaction outside the host active results in nitro reduction *via* $1e^-$ transfer events.

From a mechanistic viewpoint, encapsulation of a substrate in a pocket forces the active sites to be in close proximity with the substrate, enabling efficient hydrogenation in the pocket and gave the oxidation state of the active sites (NAD^+ mimics) (Figure S23).⁴¹ Under illumination, the oxidation state NAD^+ mimics were regenerated *via* photoinduced electron transfer from electron donors outside the flask (Figures 5 and S18).^{37,42} DFT calculations were further performed to determine the molar free energy changes of the $2e^-$ hydride transfer hydrogenation and $1e^-$ transfer

$\text{Ir}(\text{ppy})_2(\text{phen})^+$ is a well-known photosensitizer that drives several photocatalytic reactions⁵¹ and exhibits a similar absorption band⁵² to that of the NAD^+ mimics with a negative redox potential in its reduced state, $\text{Ir}(\text{ppy})_2(\text{phen})$. The luminescent titration of $\text{Ir}(\text{ppy})_2(\text{phen})^+$ upon the addition of **1**, the electron donors $\text{HCOOH}/\text{Et}_3\text{N}$ and Zn-FPB with the same concentrations used in the reaction condition suggested that a photoinduced electron transfer from $\text{Ir}(\text{ppy})_2(\text{phen})^+$ to **1** dominated the excited quenching processes (Figures S24–S27). The addition of $\text{Ir}(\text{ppy})_2(\text{phen})^+$ (1.0 mM) in the aforementioned reaction mixture gave the major product **1b** in a 64% yield with a 22% yield of the minor product **1a**. When decreasing the reaction concentration of **1** (2.5 $\mu\text{mol}/\text{time}$, ten times), the photoinduced electron transfer from the electron donors $\text{HCOOH}/\text{Et}_3\text{N}$ to $\text{Ir}(\text{ppy})_2(\text{phen})^+$ dominated the excited quenching processes to give reduced $\text{Ir}(\text{ppy})_2(\text{phen})$,⁵¹ which further reduced the catalyst Zn-FPB and **1**.⁵³ The major product was **1b** in a decreased yield of 54%, and the yield of the minor product **1a** increased to 33% (Figure 7a).

Ni-FPB (Figures 7c and S7) as a catalyst yielded 81% of **1a** with a high selectivity greater than 99% in the presence of $\text{HCOOH}/\text{Et}_3\text{N}$ as a reductant and the addition of $\text{Ir}(\text{ppy})_2(\text{phen})^+$ (1.0 mM) to the reaction mixture decreased the yield of **1a** to 18% with a **1b** yield of 70% (Table S14). Lower the reaction concentration of **1** (2.5 $\mu\text{mol}/\text{time}$, ten times) to decrease the quenching process of **1** on the photosensitizer (Figures S27 and S28) and the reaction rate outside the molecular flask, the reduced $\text{Ir}(\text{ppy})_2(\text{phen})$ reduced the redox active metal ions in the host, which further enhanced regeneration of NADH mimics. The major product was switched to **1a** with a yield of 71% and selectivity of more than 85% (Figure 6b) by the carefully regulating the reaction kinetics inside and outside the host from

the influences of the thermodynamically favored hydrogenation groups. The results indicated that this simple approach to localize and differentiate $2e^-$ and $1e^-$ hydrogenation pathways inside and outside the pocket could comfortably tuned the selectivity of the two functional groups in bifunctional chemicals. Clearly, the selectivity of the hydrogenation product towards **1a** and **1b** can be directly switched *via* varying the substrate concentration (Figure S29). A control experiment based on the molecular flask Ni-FPB (Figures 1d, S6 and S8) that resembles both the coordination geometry of the nickel(II) ion and the molecular square but with a central benzene ring replacing the center ring of the NADH mimics gave an over 80% selectivity of **1b** under the same conditions in the presence of $\text{Ir}(\text{ppy})_2(\text{phen})^+$, even lower the reaction concentration of **1** (Figure S30 and Table S14). The absence of NADH mimics prevents any switchable possibility of selectivity. Such a switching approach could be also extended to the redox-active hosts containing $\text{Co}(\text{II})$ and $\text{Fe}(\text{II})$ ions (Figures 7d, 7e, S9 and S10). The differences in the selectivity for **1a** over **1b** even in the presence of a photosensitizer suggested that the electron donating ability to the redox-active metal ions, in addition to the NAD^+ mimics, is an important factor influenced the *in situ* regeneration of the active sites, the conversion and the hydrogenation selectivity (Figures S31, S32 and Table S14). A simple comparison of the selectivity of **1a** with the redox potentials of these molecular squares further confirmed that the direct electron transfer from the reduction state of the photosensitizer outside the pocket to the catalyst hosts dominates the *in situ* generation of the active sites (Figure S17).

39 (*p*-nitroso)nitrobenzene) which contains two reducing groups with different electron transfer pathways was selected as another typical substrate, to demonstrate the broader applicability

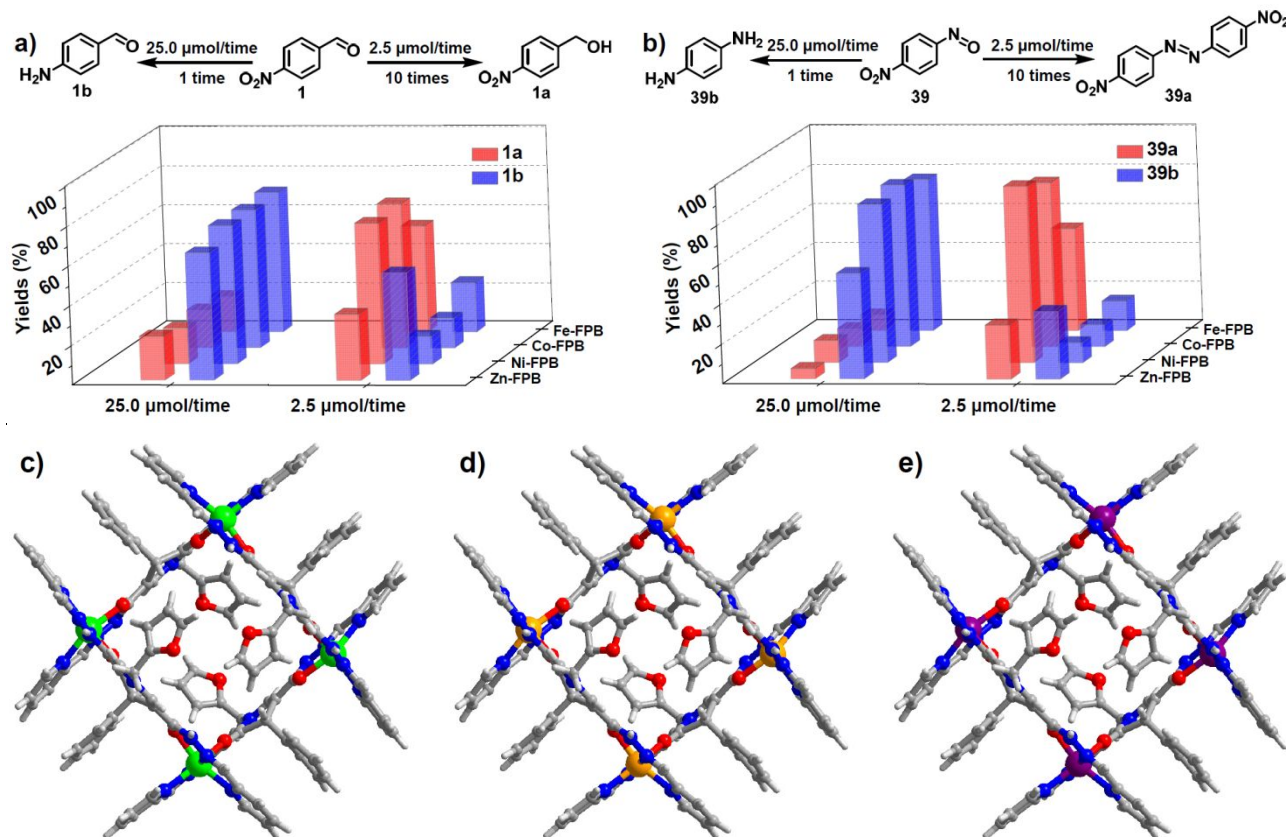


Figure 7. Switchable selectivity of the photocatalytic transfer hydrogenation: Yields of (d) 4-nitrophenylmethanol (**1a**, red) and 4-aminobenzaldehyde (**1b**, blue) by the system containing substrate **1** (5.0 mM), catalysts (0.1 mM), $\text{HCOOH}/\text{Et}_3\text{N}$ (0.1/0.05 M), NaBH_3CN (1.0 mM) and of (e) 1,2-bis(4-nitrophenyl)diazene (**39a**, red) and ursol (**39b**, blue) by the system containing substrate **39** (5.0 mM), catalysts (0.1 mM), $\text{HCOOH}/\text{Et}_3\text{N}$ (0.1/0.05 M) and NaBH_3CN (1.0 mM) in a $\text{CH}_3\text{CN}/\text{H}_2\text{O}$ solution (1:1, $\text{pH} = 8.50$) under 420 nm illumination. Crystal structures of the macrocycle Ni-FPB (c), Co-FPB (d) and Fe-FPB (e) with NADH -mimicking ligands. Anions and solvent molecules are omitted for clarity. Ni green, Co orange, Fe violet, O red, N blue, C grey and H white.

of the approach (Figure S33). Generally, the reduction of a nitro group to an amino group requires six electrons and six protons.⁵⁴ The reduction of a nitro group to a nitroso group and a hydroxylamine to an amino were through a $1e^-$ transfer hydrogenation process, whereas the reduction of nitroso to hydroxylamine occurs through a $2e^-$ hydride transfer hydrogenation.⁵⁵ In the absence of the photosensitizer, 1,2-bis(4-nitrophenyl)diazene (**39a**)⁵⁶ was obtained with a selectivity above 99% (Table S15). The substrate **39** (5.0 mM) was added to the solution containing Ir(ppy)₂(phen)⁺ (1.0 mM), and ursol (**39b**), was obtained with an 80% yield. Lower the reaction concentration of **39** (2.5 μmol/time, ten times), an 89% yield of **39a** with a 90% selectivity was achieved after 6h (Figure 7b). Because **39a** was formed by mixing a nitroso group with hydroxylamine in solution, the switchable selectivity should be attributed to the selective reduction of the nitro group through a $1e^-$ electron transfer process outside the flask, whereas the reduction of the nitroso group is through a $2e^-$ hydride transfer hydrogenation inside the flask (Figures 8 and S34).

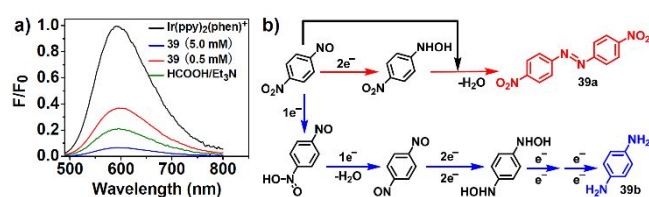


Figure 8. (a) Normalized fluorescence of Ir(ppy)₂(phen)⁺ (1.0 mM, black line) and of the aforementioned solution upon addition of **39** (0.5 mM, red line), **39** (5.0 mM, blue line) or HCOOH/Et₃N (0.1/0.05 M, green line). (b) The selective hydrogenation pathways of the *p*-(nitroso)nitrobenzene.

In summary, by incorporating NADH active sites into metal-organic hosts to localize the hydrogenation events inside and outside the pocket, we establish a new approach for modifying $2e^-$ hydride transfer hydrogenation and $1e^-$ transfer hydrogenation pathways to control and switch the selectivity between C=X (X = O, N) groups and nitro groups in bifunctional compounds. Inside the molecular flask, the NADH active sites highly selectively reduce the C=X (X = O, N) groups in the pocket *via* a typical $2e^-$ hydride transfer hydrogenation, and the formed excited-state NAD⁺ mimics oxidize the reductant *via* two consecutive $1e^-$ processes to regenerate the NADH active sites under illumination. Outside the molecular flask, electron donors in the ground state or in the excited state highly selectively reduce nitro groups through a typical $1e^-$ hydrogenation process. Notably, the selectivity of hydrogenation of bifunctional compounds could be switched by simply regulating the reaction kinetics of the two hydrogenation pathways, *i.e.*, varying the concentrations of the substrate and electron donor, because the kinetics inside the pocket are controlled only by the concentration of the host-guest complex and not directly by the concentration of the substrate. Thus, this method represents a new synthetic platform for the designation of novel photocatalysis. Compared to other reported transfer hydrogenation approaches, our approach of localizing the NADH-cofactor-derived biomimetic $2e^-$ hydride transfer hydrogenation pathway inside a molecular flask to control the electron transfer pathway and high selectivity of the product is quite significant, representing an unexplored intersection of group-selective syntheses, catalysis with earth-abundant metals, photoinduced processes, and transfer hydrogenation, which each represents an important current theme in chemical synthesis.

EXPERIMENTAL SECTION

Synthesis of H₂FPB: Compound 1-(furan-2-ylmethyl)-4-phenyl-1,4-dihydropyridine-3,5-dicarbohydrazide (3.53 g, 10 mmol) was added to an ethanol solution (50 mL) containing 2-pyridylaldehyde (2.35 g, 22 mmol). After 5 drops of acetic acid was added, the mixture was heated at 85°C under magnetic stirring for 12 h according to the reference. The yellow solid was collected by filtration, washed with methanol and dried in vacuum. Yield: 3.29 g, 65.6%. ¹H NMR (400 MHz, DMSO-*d*₆, ppm): δ 11.38 (s, 2H), 8.57 (d, *J* = 4.4 Hz, 2H), 8.24 (s, 2H), 7.84 (m, 4H), 7.75 (s, 1H), 7.47 (s, 2H), 7.37 (m, 2H), 7.24 (m, 4H), 7.11 (t, *J* = 7.2 Hz, 1H), 6.52 (s, 2H), 5.33 (s, 1H), 4.76 (s, 2H). ¹³C NMR (101 MHz, DMSO-*d*₆, ppm) δ 163.9, 153.5, 150.6, 149.4, 146.4, 145.3, 143.5, 136.7, 135.2, 128.1, 127.6, 126.2, 124.0, 119.6, 110.7, 109.3, 108.8, 50.1, 36.1. Elemental analysis calcd for C₃₀H₂₅N₇O₃: H 4.74, C 67.79, N 18.44%. Found: H 4.82, C 67.01, N 18.21%. ESI-MS calcd for C₃₀H₂₅N₇O₃ 531.2019, found 532.2088 [M+H]⁺ (100%), 554.1927 [M+Na]⁺ (8%).

Synthesis of H₂FMB: Compound 5-(furan-2-ylmethyl)isophthalohydrazide (2.84 g, 10 mmol) was added to an ethanol solution (50 mL) containing 2-pyridylaldehyde (2.35 g, 22 mmol). After 5 drops of acetic acid was added, the mixture was heated at 85 °C under magnetic stirring for 12 h according to the reference. The yellow solid was collected by filtration, washed with methanol and dried in vacuum. Yield: 3.82 g, 83%. ¹H NMR (400 MHz, DMSO-*d*₆, ppm): δ 12.24 (s, 2H), 8.64 (d, *J* = 4.4 Hz, 2H), 8.51 (s, 2H), 8.37 (s, 1H), 8.02 (m, 4H), 7.90 (t, *J* = 7.6 Hz, 2H), 7.58 (s, 1H), 7.44 (t, *J* = 6.4 Hz, 2H), 6.41 (s, 1H), 6.24 (s, 1H), 4.18 (s, 2H). ¹³C NMR (101 MHz, DMSO-*d*₆, ppm) δ 162.7, 153.2, 153.1, 149.5, 148.5, 142.2, 139.4, 136.9, 133.8, 131.3, 125.1, 124.5, 120.0, 110.6, 106.8, 33.3. Elemental analysis calcd for C₂₅H₂₀N₆O₃: H 4.46, C 66.36, N 18.57%. Found: H 4.56, C 65.57, N 18.41%. ESI-MS calcd for C₂₅H₂₀N₆O₃ 452.1597, found 453.1681 [M+H]⁺ (100%), 475.1476 [M+Na]⁺ (9%).

Preparation of Zn-FPB: Zn(BF₄)₂·6H₂O (34.7 mg, 0.10 mmol) and H₂FPB (53.2 mg, 0.10 mmol) were dissolved in CH₃CN to give a yellow solution. The solution was diffused with ether for several days at room temperature to give X-ray quality yellow block crystals. Yield: 68%. ¹H NMR (400 MHz, DMSO-*d*₆, ppm): δ 12.00 (s, 2H), 8.53 (s, 2H), 8.33 (s, 2H), 7.93 (m, 4H), 7.76 (s, 1H), 7.61 (s, 2H), 7.51 (s, 2H), 7.22 (m, 4H), 7.12 (m, 1H), 6.53 (s, 2H), 5.29 (s, 1H), 4.84 (s, 2H). Elemental analysis calcd for Zn₄(C₃₀H₂₄N₇O₃)₄·4BF₄·2CH₃CN: H, 3.65; C, 52.94; N, 14.94%. Found: H, 3.68; C, 52.77; N, 14.88%. ESI-MS: *m/z*: 793.8252 [H₃Zn₄(FPB)₄]³⁺ (100%), 1190.2319 [H₂Zn₄(FPB)₄]²⁺ (78%).

Preparation of Zn-FPB ⊃ 1: Zn(CF₃SO₃)₂ (36.1 mg, 0.10 mmol), H₂FPB (53.2 mg, 0.10 mmol) and 4-nitrobenzaldehyde (37.8 mg, 0.25 mmol) were dissolved in CH₃CN to give a yellow solution. The solution was diffused with ether for several days at room temperature to give X-ray quality yellow block crystals. Yield: 38%. Elemental analysis calcd for Zn₄(C₃₀H₂₅N₇O₃)₄·8CF₃SO₃·C₇H₅NO₃·2CH₃CN: H, 2.93; C, 43.78; N, 11.39%. Found: H, 2.95; C, 43.69; N, 11.37%. ESI-MS: *m/z*: 844.1558 [H₃Zn₄(FPB)₄ ⊃ (1)]³⁺ (25%), 1265.7304 [H₂Zn₄(FPB)₄ ⊃ (1)]²⁺ (24%).

Preparation of Fe-FPB: Fe(ClO₄)₂·6H₂O (36.3 mg, 0.10 mmol) and H₂FPB (53.2 mg, 0.10 mmol) were dissolved in CH₃CN to give a yellow solution. The solution was diffused with ether for several days at room temperature to give X-ray quality purple block crystals. Yield: 54%. Elemental analysis calcd for Fe₄(C₃₀H₂₄N₇O₃)₄·6ClO₄·CH₃CN: H, 3.41; C, 49.08; N, 13.61%. Found: H, 3.43; C, 48.97; N, 13.57%. ESI-MS: *m/z*: 785.5038 [H₃Fe₄(FPB)₄]³⁺ (69%), 1171.7513 [H₂Fe₄(FPB)₄]²⁺ (100%).

Preparation of Co-FPB: Co(BF₄)₂·6H₂O (34.0 mg, 0.10 mmol) and H₂FPB (53.2 mg, 0.10 mmol) were dissolved in CH₃CN to give a yellow solution. The solution was diffused with ether for several days at room temperature to give X-ray quality red block crystals. Yield: 33%. Elemental analysis calcd for Co₄(C₃₀H₂₄N₇O₃)₄·4BF₄: H, 3.58; C, 53.28; N, 14.50%. Found: H, 3.61; C, 53.12; N, 14.46%. ESI-MS: *m/z*: 785.4830 [H₃Co₄(FPB)₄]³⁺ (100%), 1177.6599 [H₂Co₄(FPB)₄]²⁺ (83%), 1231.2565 [H₃Co₄(FPB)₄·BF₄]²⁺ (40%).

Preparation of Ni-FPB: Ni(ClO₄)₂·6H₂O (36.5 mg, 0.10 mmol) and H₂FPB (54.2 mg, 0.10 mmol) were dissolved in CH₃CN to give a yellow solution. The solution was diffused with ether for several days at room temperature to give X-ray quality yellow block crystals. Yield: 56%. Elemental analysis calcd for Ni₄(C₃₀H_{24.5}N₇O₃)₄·6ClO₄·2CH₃CN: H, 3.45; C, 49.03; N, 13.83%. Found: H, 3.46; C, 48.95; N, 13.81%. ESI-MS: *m/z*: 785.1693 [H₃Ni₄(FPB)₄]³⁺ (100%), 1177.2492 [H₂Ni₄(FPB)₄]²⁺ (53%).

Preparation of Ni-FMB: Ni(ClO₄)₂·6H₂O (36.5 mg, 0.10 mmol) and H₂FMB (46.3 mg, 0.10 mmol) were dissolved in CH₃CN/C₂H₅OH (v:v = 9:1) to give a yellow solution. The solution was diffused with ether for several days at room temperature to give X-ray quality light yellow block crystals. Yield: 21%. Elemental analysis calcd for Ni₄(C₂₅H_{19.5}N₆O₃)₄·6ClO₄·CH₃CN·3H₂O: H, 3.21; C, 44.80; N, 12.81%. Found: H, 3.24; C, 44.65; N, 12.77%. ESI-MS: *m/z*: 679.7817 [H₃Ni₄(FMB)₄]³⁺ (100%), 1019.1665 [H₂Ni₄(FMB)₄]²⁺ (76%).

Single crystal X-ray crystallography: The intensities were collected on a Bruker SMART APEX CCD diffractometer equipped with a graphite-monochromated Mo-K α (λ = 0.71073 Å) radiation source; the data were acquired using the SMART and SAINT programs.^{57,58} The structures were solved by direct methods and refined on *F*² by full-matrix least-squares methods using the SHELXTL version 5.1 software.⁵⁹

In the structural refinement of Zn-FPB, except one partly occupied solvent CH₃CN molecule and all the fluorine atoms of a disordered BF₄⁻ anion, all the non-hydrogen atoms were refined anisotropically. Hydrogen atoms within the ligand backbones and the solvent CH₃CN molecule were fixed geometrically at calculated distances and allowed to ride on the parent non-hydrogen atoms. To assist the stability of refinements, the furan and benzene rings in the ligand, BF₄⁻ anions and solvent CH₃CN molecule were restrained as idealized regular polygons and thermal parameters on adjacent atoms in furan and benzene rings were restrained to be similar. All the fluorine atoms of a BF₄⁻ anion were disordered into two parts with the *s.o.f* of each part being fixed at free values. The SQUEEZE subroutine in PLATON was used⁶⁰.

In the structural refinement of Zn-FPB \supset **1**, except one partly occupied solvent CH₃CN molecule and one partly occupied solvent water molecule, all the carbon and fluorine atoms of a disordered CF₃SO₃⁻ anions and substrate 4-nitrobenzaldehyde, all the non-hydrogen atoms were refined anisotropically. Hydrogen atoms within the ligand backbones, substrate and the solvent CH₃CN molecules were fixed geometrically at calculated distances and allowed to ride on the parent non-hydrogen atoms. To assist the stability of refinements, one furan ring in the ligands, substrate, one CF₃SO₃⁻ anion and one solvent CH₃CN molecule were restrained as idealized regular polygons and thermal parameters on adjacent atoms in furan ring and substrate were restrained to be similar. All the carbon and fluorine atoms of a CF₃SO₃⁻ anion were disordered into two parts with the *s.o.f* of each part being fixed at free values.

In the structural refinement of Fe-FPB, except one partly occupied solvent CH₃CN molecule and all the oxygen atoms of a

disordered ClO₄⁻ anion, all the non-hydrogen atoms were refined anisotropically. Hydrogen atoms within the ligand backbones and the solvent CH₃CN molecule were fixed geometrically at calculated distances and allowed to ride on the parent non-hydrogen atoms. To assist the stability of refinements, the furan and benzene rings in the ligand, ClO₄⁻ anions and solvent CH₃CN molecule were restrained as idealized regular polygons and thermal parameters on adjacent atoms in solvent CH₃CN molecule, partly disordered oxygen atoms of a ClO₄⁻ anion, furan and benzene rings were restrained to be similar. All the oxygen atoms of a ClO₄⁻ anion were disordered into two parts with the *s.o.f* of each part being fixed at free values. The SQUEEZE subroutine in PLATON was used⁶⁰.

In the structural refinement of Co-FPB, except two partly occupied BF₄⁻ anions, all the non-hydrogen atoms were refined anisotropically. Hydrogen atoms within the ligand backbones were fixed geometrically at calculated distances and allowed to ride on the parent non-hydrogen atoms. To assist the stability of refinements, the furan and benzene rings in the ligand and BF₄⁻ anions were restrained as idealized regular polygons and thermal parameters on adjacent atoms in partly disordered fluorine atoms of two BF₄⁻ anions, furan and benzene rings were restrained to be similar. All the fluorine atoms of two BF₄⁻ anions were disordered into two parts with the *s.o.f* of each part being fixed at free values. The SQUEEZE subroutine in PLATON was used⁶⁰.

In the structural refinement of Ni-FPB, except two partly occupied solvent CH₃CN molecules and all the oxygen atoms of a disordered ClO₄⁻ anion, all the non-hydrogen atoms were refined anisotropically. Hydrogen atoms within the ligand backbones and the solvent CH₃CN molecule were fixed geometrically at calculated distances and allowed to ride on the parent non-hydrogen atoms. To assist the stability of refinements, the furan and benzene rings in the ligand, one ClO₄⁻ anion and two solvent CH₃CN molecules were restrained as idealized regular polygons and thermal parameters on adjacent atoms in furan and benzene rings were restrained to be similar. All the oxygen atoms of a ClO₄⁻ anion were disordered into two parts with the *s.o.f* of each part being fixed at free values. The SQUEEZE subroutine in PLATON was used⁶⁰.

In the structural refinement of Ni-FMB, except some solvent water molecules, all the non-hydrogen atoms were refined anisotropically. Hydrogen atoms within the ligand backbones, the solvent CH₃CN, ether and ethanol molecule were fixed geometrically at calculated distances and allowed to ride on the parent non-hydrogen atoms. To assist the stability of refinements, two furan rings and one benzene ring in the ligands, ClO₄⁻ anions and solvent CH₃CN, ether and ethanol molecules were restrained as idealized regular polygons and thermal parameters on adjacent atoms in furan rings were restrained to be similar. The furan and benzene rings in one ligand were disordered into two parts with the *s.o.f* of each part being fixed at free values. All the oxygen atoms of three ClO₄⁻ anions were disordered into two parts with the *s.o.f* of each part being fixed at free values.

Photocatalytic transfer hydrogenation protocol. The catalyst (0.1 mM, 0.5 μ mol), substrates (5.0 mM, 25.0 μ mol), NaBH₃CN (1.0 mM, 5.0 μ mol) and HCOOH/Et₃N (0.1/0.05 M, 0.5/0.25 mmol) in CH₃CN/H₂O (1:1 in volume) were added to obtain a total volume of 5.0 mL in a 20 mL flask. The flask was degassed by bubbling argon for 15 min under atmospheric pressure at room temperature. The pH (= 8.5) of this solution was adjusted to a specific pH by adding H₂SO₄ or NaOH and measured with a pH meter. After that, the samples were irradiated by a 100 W LED Lamp at 420 nm, the reaction temperature was 298 K by using a water filter to absorb heat. The yields were determined by ¹H-NMR analysis of the crude products.

ASSOCIATED CONTENT

Supporting Information

The Supporting Information is available free of charge on the ACS Publications website.

Complete experimental details and supporting Figures.

X-ray data for Zn-FPB (CCDC 1891712);

X-ray data for Zn-FPB \supset 1 (CCDC 1891711);

X-ray data for Fe-FPB (CCDC 1891710);

X-ray data for Co-FPB (CCDC 1891708);

X-ray data for Ni-FPB (CCDC 1891709);

X-ray data for Ni-FMB (CCDC 1906243);

AUTHOR INFORMATION

Corresponding Author

*zhaol@dlut.edu.cn

*cyduan@dlut.edu.cn

ORCID

Liang Zhao: 0000-0001-8197-6686

Cheng He: 0000-0002-1426-0124

Joost N. H. Reek: 0000-0001-5024-508X

Chunying Duan: 0000-0003-1638-6633

Notes

The authors declare no competing financial interests.

ACKNOWLEDGMENT

This work was supported by the National Natural Science Foundation of China (21531001, 21820102001 and 21861132004). We thank the Shenzhen HUASUAN Technology Co., Ltd., for performing the DFT calculations and data analysis.

REFERENCES

- Wang, D.; Astruc, D. The golden age of transfer hydrogenation. *Chem. Rev.* **2015**, *115*, 6621–6686.
- Soldevila-Barreda, J. J.; Romero-Canelon, I.; Habtemariam, A.; Sadler, P. J. Transfer hydrogenation catalysis in cells as a new approach to anticancer drug design. *Nat. Commun.* **2015**, *6*, 6582.
- Zhu, C.; Saito, K.; Yamanaka, M.; Akiyama, T. Benzothiazoline: versatile hydrogen donor for organocatalytic transfer hydrogenation. *Acc. Chem. Res.* **2015**, *48*, 388–398.
- Coverdale, J. P. C.; Romero-Canelón, I.; Sanchez-Cano, C.; Clarkson, G. J.; Habtemariam, A.; Wills, M.; Sadler, P. J. Asymmetric transfer hydrogenation by synthetic catalysts in cancer cells. *Nat. Chem.* **2018**, *10*, 347–354.
- Touge, T.; Nara, H.; Fujiwhara, M.; Kayaki, Y.; Ikariya, T. Efficient access to chiral benzhydrols via asymmetric transfer hydrogenation of unsymmetrical benzophenones with bifunctional oxo-tethered ruthenium catalysts. *J. Am. Chem. Soc.* **2016**, *138*, 10084–10087.
- Zuo, W.; Lough, A. J.; Li, Y. F.; Morris, R. H. Amine(imine) diphosphine iron catalysts for asymmetric transfer hydrogenation of ketones and imines. *Science* **2013**, *342*, 1080–1083.
- Zhao, M.; Yuan, K.; Wang, Y.; Li, G.; Guo, J.; Gu, L.; Hu, W.; Zhao, H.; Tang, Z. Metal-organic frameworks as selectivity regulators for hydrogenation reactions. *Nature* **2016**, *539*, 76–80.
- Yuan, K.; Song, T.; Wang, D.; Zhang, X.; Gao, X.; Zou, Y.; Dong, H.; Tang, Z.; Hu, W. Effective and selective catalysts for cinnamaldehyde hydrogenation: hydrophobic hybrids of metal-organic frameworks, metal nanoparticles, and micro- and mesoporous polymers. *Angew. Chem. Int. Ed.* **2018**, *57*, 5708–5713.
- Ilic, S.; Alherz, A.; Musgrave, C. B.; Glusac, K. D. Thermodynamic and kinetic hydricities of metal-free hydrides. *Chem. Soc. Rev.* **2018**, *47*, 2809–2836.
- Zheng, C.; You, S. L. Transfer hydrogenation with Hantzsch esters and related organic hydride donors. *Chem. Soc. Rev.* **2012**, *41*, 2498–2518.
- Zhang, P.; Yuly, J. L.; Lubner, C. E.; Mulder, D. W.; King, P. W.; Peters, J. W.; Beratan, D. N. Electron Bifurcation: Thermodynamics and kinetics of two-electron brokering in biological redox chemistry. *Acc. Chem. Res.* **2017**, *50*, 2410–2417.
- Buckel, W.; Thauer, R. K. Flavin-based electron bifurcation, a new mechanism of biological energy coupling. *Chem. Rev.* **2018**, *118*, 3862–3886.
- Cook, T. R.; Stang, P. J. Recent developments in the preparation and chemistry of metallacycles and metallacages via coordination. *Chem. Rev.* **2015**, *115*, 7001–7045.
- Brown, C. J.; Toste, F. D.; Bergman, R. G.; Raymond, K. N. Supramolecular catalysis in metal-ligand cluster hosts. *Chem. Rev.* **2015**, *115*, 3012–3035.
- Jiao, J.; Tan, C.; Li, Z.; Liu, Y.; Han, X.; Cui, Y., Design and Assembly of Chiral Coordination Cages for Asymmetric Sequential Reactions. *J. Am. Chem. Soc.* **2018**, *140*, 2251–2259.
- Ward, M. D.; Hunter, C. A.; Williams, N. H., Coordination Cages Based on Bis(pyrazolylpyridine) Ligands: Structures, Dynamic Behavior, Guest Binding, and Catalysis. *Acc. Chem. Res.* **2018**, *51*, 2073–2082.
- Zhao, L.; Jing, X.; Li, X.; Guo, X.; Zeng, L.; He, C.; Duan, C., Catalytic properties of chemical transformation within the confined pockets of Werner-type capsules. *Coord. Chem. Rev.* **2019**, *378*, 151–187.
- Jing, X.; Yang, Y.; He, C.; Chang, Z.; Reek, J. N. H.; Duan, C. Control of redox events by dye encapsulation applied to light-driven splitting of hydrogen sulfide. *Angew. Chem. Int. Ed.* **2017**, *56*, 11759–11763.
- Salles, Jr.; A. G.; Zarra, S.; Turner, R. M.; Nitschke, J. R. A self-organizing chemical assembly line. *J. Am. Chem. Soc.* **2013**, *135*, 19143–19146.
- Wang, Z. J.; Clary, K. N.; Bergman, R. G.; Raymond, K. N.; Toste, F. D. A supramolecular approach to combining enzymatic and transition metal catalysis. *Nat. Chem.* **2013**, *5*, 100–103.
- Ueda, Y.; Ito, H.; Fujita, D.; Fujita, M., Permeable Self-Assembled Molecular Containers for Catalyst Isolation Enabling Two-Step Cascade Reactions. *J. Am. Chem. Soc.* **2017**, *139*, 6090–6093.
- Dhers, S.; Mondal, A.; Aguilà, D.; Ramírez, J.; Vela, S.; Dechambenoit, P.; Rouzières, M.; Nitschke, J. R.; Clérac, R.; Lehn, J.-M. Spin state chemistry: modulation of ligand pKa by spin state switching in a [2x2] iron(ii) grid-type complex. *J. Am. Chem. Soc.* **2018**, *140*, 8218–8227.
- Cullen, W.; Metherell, A. J.; Wragg, A. B.; Taylor, C. G. P.; Williams, N. H.; Ward, M. D., Catalysis in a Cationic Coordination Cage Using a Cavity-Bound Guest and Surface-Bound Anions: Inhibition, Activation, and Autocatalysis. *J. Am. Chem. Soc.* **2018**, *140*, 2821–2828.
- Rizzuto, F. J.; Nitschke, J. R. Stereochemical plasticity modulates cooperative binding in a Co(II)₁₂L₆ cuboctahedron. *Nat. Chem.* **2017**, *9*, 903–908.
- Trickett, C. A.; Osborn Popp, T. M.; Su, J.; Yan, C.; Weisberg, J.; Huq, A.; Urban, P.; Jiang, J.; Kalmutzki, M. J.; Liu, Q.; Baek, J.; Head-Gordon, M. P.; Somorjai, G. A.; Reimer, J. A.; Yaghi, O. M., Identification of the strong Brønsted acid site in a metal-organic framework solid acid catalyst. *Nat. Chem.* **2019**, *11*, 170–176.
- Bocokic, V.; Kalkan, A.; Lutz, M.; Spek, A. L.; Gryko, D. T.; Reek, J. N., Capsule-controlled selectivity of a rhodium hydroformylation catalyst. *Nat. Commun.* **2013**, *4*, 2670.
- Cullen, W.; Takezawa, H.; Fujita, M., Demethylenation of Cyclopropanes via Photoinduced Guest-to-Host Electron Transfer in an M₆L₄ Cage. *Angew. Chem. Int. Ed.* **2019**, *58*, 9171–9173.
- Liu, Y.; Lee, J.; Perez, L.; Gill, A. D.; Hooley, R. J.; Zhong, W., Selective Sensing of Phosphorylated Peptides and Monitoring Kinase and Phosphatase Activity with a Supramolecular Tandem Assay. *J. Am. Chem. Soc.* **2018**, *140*, 13869–13877.
- Shi, B.; Liu, Y.; Zhu, H.; Vanderlinden, R. T.; Shangguan, L.; Ni, R.; Acharyya, K.; Tang, J. H.; Zhou, Z.; Li, X.; Huang, F.; Stang, P. J., Spontaneous Formation of a Cross-Linked Supramolecular Polymer Both in the Solid State and in Solution, Driven by Platinum(II) Metallacycle-Based Host-Guest Interactions. *J. Am. Chem. Soc.* **2019**, *141*, 6494–6498.

- 1
2
3
4
5
6
7
8
9
10
11
12
13
14
15
16
17
18
19
20
21
22
23
24
25
26
27
28
29
30
31
32
33
34
35
36
37
38
39
40
41
42
43
44
45
46
47
48
49
50
51
52
53
54
55
56
57
58
59
60
30. Nurttala, S. S.; Brenner, W.; Mosquera, J.; Vliet, K. M.; Nitschke, J. R.; Reek, J. N. H. Size-selective hydroformylation by a rhodium catalyst confined in a supramolecular cage. *Chem. Eur. J.* **2019**, *25*, 609–620.
31. Pan, M.; Wu, K.; Zhang, J. H.; Su, C. Y., Chiral metal–organic cages/containers (MOCs): From structural and stereochemical design to applications. *Coord. Chem. Rev.* **2019**, *378*, 333–349.
32. Bauer, H.; Alonso, M.; Färber, C.; Elsen, H.; Pahl, J.; Causero, A.; Ballmann, G.; Proft, F. D.; Harder, S. Imine hydrogenation with simple alkaline earth metal catalysts. *Nat. Catal.* **2018**, *1*, 40–47.
33. Popov, V. O.; Lamzin, V. S. NAD⁺-dependent formate dehydrogenase. *Biochem. J.* **1994**, *301*, 625–643.
34. Ranasinghe, C.; Guo, Q.; Sapienza, P. J.; Lee, A. L.; Quinn, D. M.; Cheatum, C. M.; Kohen, A., Protein Mass Effects on Formate Dehydrogenase. *J. Am. Chem. Soc.* **2017**, *139*, 17405–17413.
35. Kaphan, D. M.; Levin, M. D.; Bergman, R. G.; Raymond, K. N.; Toste, F. D. A supramolecular microenvironment strategy for transition metal catalysis. *Science* **2015**, *350*, 1235–1238.
36. Jongkind, L. J.; Elemans, J.; Reek, J. N. H., Cofactor Controlled Encapsulation of a Rhodium Hydroformylation Catalyst. *Angew. Chem. Int. Ed.* **2017**, *56*, 2696–2699.
37. Zhao, L.; Wei, J.; Lu, J.; He, C.; Duan, C. Renewable molecular flasks with NADH models: combination of light-driven proton reduction and biomimetic hydrogenation of benzoxazinones. *Angew. Chem. Int. Ed.* **2017**, *56*, 8692–8696.
38. Sigurskjold, B. W., Exact Analysis of Competition Ligand Binding by Displacement Isothermal Titration Calorimetry. *Anal. Biochem.* **2000**, *277*, 260–266.
39. Christensen, T.; Gooden, D. M.; Kung, J. E.; Toone, E. J., Additivity and the Physical Basis of Multivalency Effects: A Thermodynamic Investigation of the Calcium EDTA Interaction. *J. Am. Chem. Soc.* **2003**, *125*, 7357–7366.
40. Zhao, L.; Wei, J.; Zhang, J.; He, C.; Duan, C., Encapsulation of a Quinhydrone Cofactor in the Inner Pocket of Cobalt Triangular Prisms: Combined Light-Driven Reduction of Protons and Hydrogenation of Nitrobenzene. *Angew. Chem. Int. Ed.* **2017**, *56*, 15284–15288.
41. McSkimming, A.; Bhadbhade, M. M.; Colbran, S. B. Bio-inspired catalytic imine reduction by rhodium complexes with tethered Hantzsch pyridinium groups: evidence for direct hydride transfer from dihydropyridine to metal-activated substrate. *Angew. Chem. Int. Ed.* **2013**, *52*, 3411–3416.
42. Wang, X.; Saba, T.; Yiu, H. H. P.; Howe, R. F.; Anderson, J. A.; Shi, J. Cofactor NAD(P)H regeneration inspired by heterogeneous pathways. *Chem.* **2017**, *2*, 621–654.
43. Hastings, C. J.; Bergman, R. G.; Raymond, K. N. Origins of large rate enhancements in the Nazarov cyclization catalyzed by supramolecular encapsulation. *Chem. Eur. J.* **2014**, *20*, 3966–3973.
44. Shtarev, D. S.; Shtareva, A. V.; Blokh, A. I.; Goncharova, P. S.; Makarevich, K. S. On the question of the optimal concentration of benzoquinone when it is used as a radical scavenger. *Appl. Phys. A: Solids Surf.* **2017**, *123*, 602.
45. Le, C.; Chen, T. Q.; Liang, T.; Zhang, P.; MacMillan, D. W. C. A radical approach to the copper oxidative addition problem: Trifluoromethylation of bromoarenes. *Science* **2018**, *360*, 1010–1014.
46. Wang, D.; Zhu, N.; Chen, P.; Lin, Z.; Liu, G., Enantioselective Decarboxylative Cyanation Employing Cooperative Photoredox Catalysis and Copper Catalysis. *J. Am. Chem. Soc.* **2017**, *139*, 15632–15635.
47. Das, S.; Bobbink, F. D.; Laurency, G.; Dyson, P. J., Metal-free catalyst for the chemoselective methylation of amines using carbon dioxide as a carbon source. *Angew. Chem. Int. Ed.* **2014**, *53*, 12876–12879.
48. Jing, J.; Huo, X.; Shen, J.; Fu, J.; Meng, Q.; Zhang, W., Direct use of allylic alcohols and allylic amines in palladium-catalyzed allylic amination. *Chem. Comm.* **2017**, *53*, 5151–5154.
49. Mamedov, V. A.; Mamedova, V. L.; Syakaev, V. V.; Korshin, D. E.; Khikmatova, G. Z.; Mironova, E. V.; Bazanova, O. B.; Rizvanov, I. K.; Latypov, S. K. Simple synthesis of 3-hydroxyquinolines via Na₂S₂O₄-mediated reductive cyclization of (2-(2-nitrophenyl)oxiran-1-yl)(aryl)methanones (*o*-nitrobenzal acetophenone oxides). *Tetrahedron* **2017**, *73*, 5082–5090.
50. Xu, H. J.; Liu, Y. C.; Fu, Y.; Wu, Y. D. Catalytic hydrogenation of α,β -epoxy ketones to form β -hydroxy ketones mediated by an NADH coenzyme model. *Org. Lett.* **2006**, *8*, 3449–3451.
51. Mills, I. N.; Porras, J. A.; Bernhard, S. Judicious design of cationic, cyclometalated Ir(III) complexes for photochemical energy conversion and optoelectronics. *Acc. Chem. Res.* **2018**, *51*, 352–364.
52. Zhao, Q.; Liu, S.; Shi, M.; Li, F.; Jing, H.; Yi, T.; Huang, C. Tuning photophysical and electrochemical properties of cationic Iridium(III) complex salts with imidazolyl substituents by proton and anions. *Organometallics* **2007**, *26*, 5922–5930.
53. Condie, A. G.; González-Gómez, J. C.; Stephenson, C. R. J. Visible-light photoredox catalysis: Aza-henry reactions via C-H functionalization. *J. Am. Chem. Soc.* **2010**, *132*, 1464–1465.
54. Blaser, H. U. A golden boost to an old reaction. *Science* **2006**, *313*, 312–313.
55. Bryant, C.; DeLuca, M. Purification and characterization of an oxygen-insensitive NAD(P)H nitroreductase from enterobacter cloacae. *J. Bio. Chem.* **1991**, *266*, 4119–4125.
56. Mondal, B.; Mukherjee, P. S. Cage encapsulated gold nanoparticles as heterogeneous photocatalyst for facile and selective reduction of nitroarenes to azo compounds. *J. Am. Chem. Soc.* **2018**, *140*, 12592–12601.
57. SMART, Data collection software (version 5.629) (Bruker AXS Inc., Madison, WI, 2003).
58. SAINT, Data reduction software (version 6.54) (Bruker AXS Inc., Madison, WI, 2003).
59. Sheldrick, G. M. SHELXTL97, Program for Crystal Structure Solution (University of Göttingen: Göttingen, Germany, 1997).
60. Spek, A. L. Single-crystal structure validation with the program PLATON. *J. Appl. Cryst.* **2003**, *36*, 7–13.

